AGU PUBLICATIONS

Journal of Advances in Modeling Earth Systems

RESEARCH ARTICLE
10.1002/2016MS000803

Key Points:
- Importance of interactive SST in idealized intraseasonal variability
- Role of vertical wind shear and radiative feedback in intraseasonal variability

Correspondence to:
U. Anber,
uanber@princeton.edu;
uanber@ldeo.columbia.edu

Citation:
Anber, U., S. Wang, and A. Sobel (2017), Coupling with ocean mixed layer leads to intraseasonal variability in tropical deep convection: Evidence from cloud-resolving simulations, *J. Adv. Model. Earth Syst.*, *9*, 616–626, doi:10.1002/2016MS000803.

Received 7 SEP 2016
Accepted 16 FEB 2017
Accepted article online 21 FEB 2017
Published online 22 MAR 2017

Coupling with ocean mixed layer leads to intraseasonal variability in tropical deep convection: Evidence from cloud-resolving simulations

Usama Anber[1], Shuguang Wang[2], and Adam Sobel[2,3]

[1]Program in Atmospheric and Oceanic Sciences, and the Geophysical Fluid Dynamics Laboratory, Princeton University, Princeton, New Jersey, USA, [2]Department of Applied Physics and Applied Mathematics, Columbia University, New York, New York, USA, [3]Lamont-Doherty Earth Observatory of Columbia University, Palisades, New York, USA

Abstract The effect of coupling a slab ocean mixed layer to atmospheric convection is examined in cloud-resolving model (CRM) simulations in vertically sheared and unsheared environments without Coriolis force, with the large-scale circulation parameterized using the Weak Temperature Gradient (WTG) approximation. Surface fluxes of heat and moisture as well as radiative fluxes are fully interactive, and the vertical profile of domain-averaged horizontal wind is strongly relaxed toward specified profiles with vertical shear that varies from one simulation to the next. Vertical wind shear is found to play a critical role in the simulated behavior. There exists a threshold value of the shear strength above which the coupled system develops regular oscillations between deep convection and dry nonprecipitating states, similar to those found earlier in a much more idealized model which did not consider wind shear. The threshold value of the vertical shear found here varies with the depth of the ocean mixed layer. The time scale of the spontaneously generated oscillations also varies with mixed layer depth, from 10 days with a 1 m deep mixed layer to 50 days with a 10 m deep mixed layer. The results suggest the importance of the interplay between convection organized by vertical wind shear, radiative feedbacks, large-scale dynamics, and ocean mixed layer heat storage in real intraseasonal oscillations.

1. Introduction

Variability in sea surface temperature (SST) regulates deep convection over tropical oceans and influences atmospheric variability on a variety of time scales. On intraseasonal time scales in particular, observational studies show the relevance of interactions between atmospheric deep convection and the ocean mixed layer, with SST anomalies generated by variations in surface turbulent and radiative fluxes [e.g., *Waliser*, 1996; *Woolnough et al*., 2000; *Vecchi and Harrison*, 2002; *Stephens et al*., 2004].

Sobel and Gildor [2003] (SG03, hereinafter) considered this problem from a theoretical point of view, using an idealized single-column model based on the Neelin-Zeng quasi-equilibrium tropical circulation model (QTCM) [*Neelin and Zeng*, 2000] coupled to a slab ocean mixed layer. Wind-evaporation and cloud-radiative feedbacks were lumped together in a single parameter, representing modulations of net surface heat flux from the ocean to the atmosphere by both processes, assuming both to be in phase with anomalies in precipitation. For some parameters, SG03 found that their model's equilibrium state was unstable to periodic oscillations whose frequency was robustly in the intraseasonal range. In addition to the parameter representing the surface flux and radiative feedbacks, the depth of the ocean mixed layer was also important, with mixed layers too shallow suppressing the oscillations and an optimum value, in the range of those observed (tens of meters) giving the strongest instability.

Maloney and Sobel [2004] (MS04, hereinafter), simulated tropical intraseasonal variability using an atmospheric general circulation model (GCM) coupled to a slab ocean mixed layer of varying depths. They found that the amplitude of intraseasonal variability in precipitation over the western Pacific was nonmonotonically sensitive to the depth of the mixed layer, reaching a maximum at 20 m, qualitatively similar to the findings of SG03 (though the amplitude of the mixed layer depth dependence was much weaker in the GCM). In the model of MS04, the wind-induced surface heat exchange (WISHE) feedback was shown to be critical. Later studies using other models (with and without ocean coupling) have suggested that radiative-

convective feedbacks are more important to intraseasonal variability than is WISHE [e.g., *Andersen and Kuang*, 2012; *Kim et al*., 2011]. *Sobel et al*. [2008, 2010] argue, following SG03, that these processes should be considered together, particularly for the purposes of comparison with other theories of intraseasonal variability that do not involve either one, but ultimately it is important to determine their relative roles if we are to understand the dynamics fully.

In this work, we report on simulations broadly similar to those of SG03, but using a cloud-resolving model to represent the atmosphere. A new element not considered in previous studies, the vertical wind shear, is found to exert an important control on the system behavior in this model. As in SG03, the effect of the large-scale dynamics is parameterized using the WTG approximation. In a previous study using a similar atmospheric model configuration with specified noninteractive radiative cooling and surface turbulent fluxes [*Anber et al*., 2014], vertical wind shear was shown to have a significant impact on both convective organization and, when surface fluxes were sufficiently strong, time-averaged and domain-averaged precipitation. In similar simulations with interactive radiation, the system was shown to experience a large increase in the gross moist stability in the presence of strong vertical shear, due to increased top-heaviness of the large-scale vertical motion profile associated with stratiform cloud [*Anber et al*., 2016].

In section 2, we describe the model and the numerical experiments. We present the results in section 3 and summarize in section 4.

2. Model Description and Experimental Design

The model used here is the Weather Research and Forecast (WRF) model version 3.3, in three spatial dimensions with doubly periodic boundary conditions. The horizontal domain size is 192×192 km^2, with a horizontal grid spacing of 2 km, and Coriolis parameter $f = 0$. There are 50 vertical levels total, with the top level at 22 km, and 10 levels in the lowest 1 km. Gravity waves propagating vertically are absorbed in the top 5 km to prevent unphysical wave reflection off the top boundary by the implicit damping vertical velocity scheme [*Klemp et al*., 2008]. The two-dimensional Smagorinsky first-order turbulent closure scheme is used to parameterize the horizontal transports by subgrid eddies. The Yonsei University (YSU) first-order closure scheme is used to parameterize nonlocal boundary layer turbulence and vertical subgrid-scale eddy diffusion [*Hong and Pan*, 1996; *Noh et al*., 2003; *Hong et al*., 2006]. The surface fluxes of moisture and heat are parameterized following Monin-Obukhov similarity theory. Microphysics is simulated using the Purdue-Lin bulk scheme [*Chen and Sun*, 2002], which has six species: water vapor, cloud water, cloud ice, rain, snow, and graupel. Radiative fluxes are determined interactively using the NCAR Community Atmosphere Model (CAM 3.0) scheme for shortwave and longwave radiation [*Collins et al*., 2004]. Diurnal and seasonal cycles are removed from the insolation so that the incoming shortwave radiative flux is constant in time.

The atmospheric model is coupled to a slab ocean mixed layer that is dynamically passive. The mixed layer temperature is predicted using the surface energy budget:

$$\rho H C \frac{dT}{dt} = -LH - SH + SW + LW \tag{1}$$

where T is sea surface temperature, ρ is water density (1000 kg m^{-3}), C is the heat capacity of water (4180 J kg^{-1} K^{-1}), H is the depth of the mixed layer, LH is the surface latent heat flux, SH is the surface sensible heat flux, SW is the net absorbed shortwave radiative flux (positive downward, W m^{-2}), and LW is the net longwave radiative flux (LW$\downarrow$ − LW$\uparrow$).

In our limited-area CRM experiments, the Weak Temperature Gradient (WTG) approximation [e.g., *Raymond and Zeng*, 2005; *Wang and Sobel*, 2011] is used to parameterize large-scale dynamics. WTG utilizes the dominant balance in the tropics between diabatic heating and adiabatic cooling (or vice versa) to determine the large-scale vertical motion field. The latter is represented by relaxing the domain mean free-tropospheric potential temperature toward a prescribed (target) reference profile over a specified time scale, at each time step:

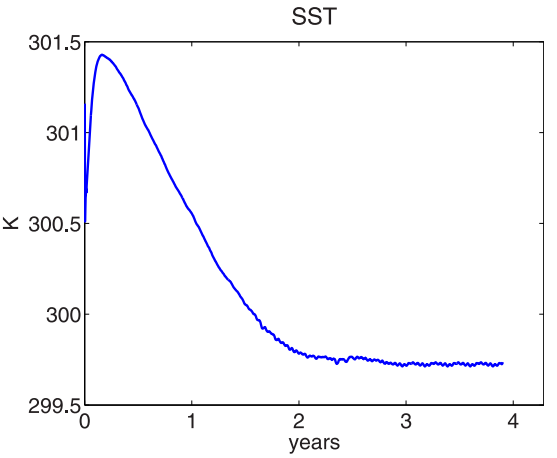

Figure 1. Time series of domain-averaged SST from RCE experiment with slab ocean mixed layer 1 m deep.

$$W_{WTG}(z) = \frac{1}{\tau}\frac{\overline{\theta}-\theta_0}{\partial\overline{\theta}/\partial z} \quad (2)$$

where W_{WTG} is the large-scale vertical velocity, $\overline{\theta}$ is the horizontal domain mean potential temperature, θ_0 is the target temperature profile, and τ is the relaxation time scale, generally interpreted as the time scale over which gravity waves propagate out of the domain, thus reducing the horizontal pressure and temperature gradients [*Bretherton and Smolarkiewicz*, 1989], here set to 3 h.

In the boundary layer, linear interpolation is applied between the magnitude of W_{WTG} at the top of the boundary layer (whose height determined internally in the model by the boundary layer scheme) and zero at the surface.

Once W_{WTG} is obtained, it is used to advect temperature and moisture vertically at each time step [e.g., *Wang and Sobel*, 2011; *Anber et al*., 2014, 2015].

Note that in WTG, unlike in radiative-convective equilibrium (RCE), surface fluxes and the vertically integrated radiative cooling are not in balance; the column budget of moist static energy (or moist entropy) includes a term representing import or export by the parameterized large-scale circulation [e.g., *Anber et al*., 2016, equation (2)], with the latter proportional to the implied mass circulation by a parameter as the gross moist stability [*Neelin and Held*, 1987; *Raymond et al*., 2009]. As a consequence, precipitation need not equal surface evaporation in steady state under WTG as it does in RCE.

We perform the following simulations:

1. RCE

   First we perform a radiative-convective equilibrium (RCE) experiment with fully interactive surface fluxes and radiative heating and no vertical shear. The incoming shortwave radiative flux at the top of the atmosphere (TOA) is set at 312.7 W m^{-2} in order to obtain a near observed value of tropical mean SST. This value is lower than the observed tropical mean insolation, and was obtained by specifying the solar constant at 491.6 W m^{-2} and the zenith angle at 50.5° in the radiation scheme, and adjusting those values until the simulation showed a time mean SST value near that observed. The magnitudes of the solar constant and the zenith angle are arbitrary and what matters is the TOA incoming radiative flux. Higher values of solar irradiance, such as that corresponding to the observed tropical mean, lead to higher values of SST. This difference may reflect biases in cloud feedbacks as well as the neglect of poleward heat transport in our RCE solutions, issues which are circumvented by reducing the solar irradiance from its observed value [e.g., *Hohenegger and Stevens*, 2016]. The depth of the mixed layer (H) is 1 m.

   The RCE experiment is run for almost 4 years, and equilibrium is achieved after approximately 3 years of integration as shown in Figure 1. The need for such a long integration is a consequence of coupling between the surface and the atmosphere, as explained by *Cronin and Emanuel* [2013]. At equilibrium, the sea surface temperature is 299.75 K, the sum of the surface latent and sensible heat fluxes is 110.14 W m^{-2}, and the mean precipitation is 3.5 mm d^{-1}. Equilibrium vertical profiles of potential temperature and moisture from this run are shown in Figures 2a and 2b, respectively, and are used to initialize the WTG experiments described below.
2. WTG

   For the WTG experiments, we set the incoming TOA shortwave flux at 405.56 W m^{-2} (solar constant of 637.6 W m^{-2} and zenith angle at 50.5°), about 90 W m^{-2} (92.88 W m^{-2} for accurate budget calculations) more than in the RCE, in order to generate a state of mean ascent similar to local tropical regions in which mean precipitation is large. The oscillations of interest here occur only in a mean state of ascent, consistent with the observed MJO which only shows large amplitude in convection in regions of mean ascent and moisture convergence, such as over the equatorial Indian and western Pacific oceans. The change of insolation is not meant to represent a global climate change, but rather to induce a change in

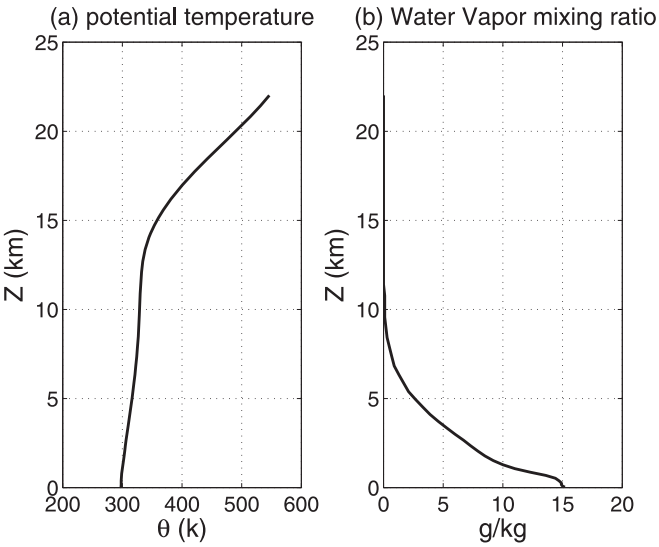

Figure 2. Vertical profiles of (a) potential temperature and (b) water vapor mixing ratio from RCE experiment at equilibrium.

local conditions (e.g., associated with moving to a different horizontal location) under a constant mean climate represented by the constant reference potential temperature profile. A similar effect could be achieved by adding a varying specified heat flux to the ocean mixed layer, for example (such as would be achieved by ocean heat transport as one moves from the eastern to western equatorial Pacific). Insolation is simply a convenient control parameter to use in order to vary the mean SST, convective intensity and large-scale vertical motion. The RCE potential temperature profile (Figure 2a) is used as the target profile against which perturbations are computed. We then run a series of these experiments for unsheared and sheared environments with different mixed layer depths of 10 cm, 1 m, and 10 m.

For the sheared environment, we impose a linear wind profile of zero at the surface and a constant, nonzero wind at the top of the shear layer, whose depth is held fixed at 12 km (exactly as in *Anber et al.* [2014, Figure 1a]). The wind at the shear layer top is in the direction of one of the coordinate axes (*x* axis here, but they are equivalent as the problem is invariant to 90° rotation), and values of 10, 15, 20, 30, and 40 m s^{-1} are used in separate experiments. The time scale over which the horizontal mean horizontal wind is relaxed toward the imposed wind profile is 1 h.

3. Results

We present results from the WTG simulations for unsheared as well as sheared flows, focusing on particular cases of sheared flow in which the solution exhibits oscillatory behavior.

3.1. Properties of the Coupled System in an Unsheared Environment

In the WTG experiment with $H = 1$ m, the SST remains almost unchanged from the RCE run at 299.8 K, despite the increase of over 90 W m^{-2} in insolation. This increase is distributed in the system as shown schematically in Figure 3. This is largely a consequence of a strong negative shortwave cloud feedback as the strength of convection increases in response to the combination of additional solar forcing and near-constant tropospheric temperature. At the top of the atmosphere, an additional 61.5 W m^{-2} (compared to the control case) of shortwave radiation is reflected due to increased cloudiness (Figure 5), while the remaining 31.4 W m^{-2} enters the coupled ocean-atmosphere system. An additional 22.7 W m^{-2} of shortwave radiation reaches the surface (after 8.7 W m^{-2} being absorbed by the atmosphere) superimposed on a 5.8 W m^{-2} increase in downward longwave, compensated by a 27.2 W m^{-2} increase in surface turbulent fluxes and a 1.2 W m^{-2} increase in upward longwave as shown in Tab1e 1. We presume the increase in surface turbulent fluxes to be a response to increased convective downdrafts in the more actively convective mean state.

Figure 4a shows mean precipitation at equilibrium as a function of the mixed layer depth. Precipitation is almost constant at 6.5 mm d^{-1} for 10 cm, 1 m, and 10 m mixed layer depth. As the surface fluxes and radiative heating are also nearly constant, as shown in Figure 4b, this implies a near-constant gross moist stability as well. For the 50 m depth mixed layer, precipitation decreases to about 3.7 mm d^{-1}. If these were truly steady solutions, the mixed layer depth should have no effect since it only appears in the tendency term in (1). However, these solutions are only statistically steady, and it is possible for the time-averaged properties to vary with the mixed layer depth since each term on the right hand side of equation (1) is itself a function

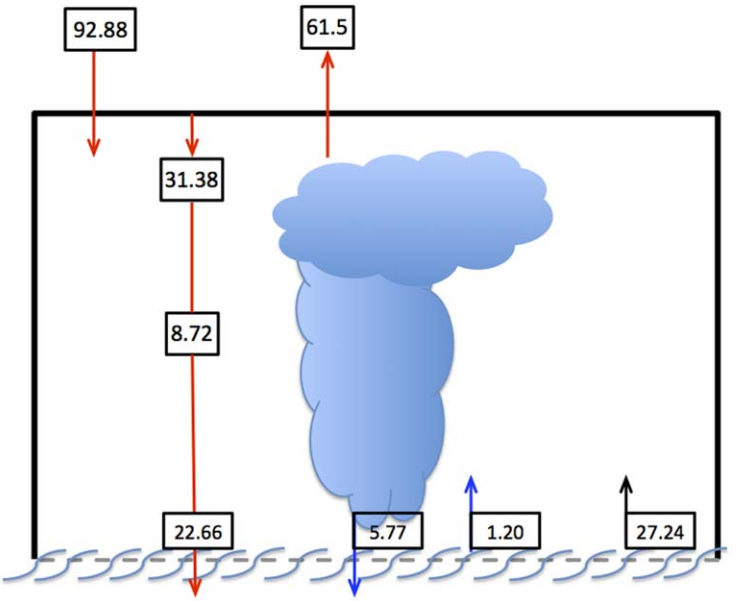

Figure 3. Schematic describing the surface, atmosphere, and top of atmosphere energy budget changes in response to the extra 92.88 W m^{-2} insolation increase from the RCE to WTG experiments. Red arrows represent shortwave radiative flux, blue longwave, and the black arrow represents surface turbulent fluxes. Units are W m^{-2}.

of SST and need not reach the same equilibrium state under different mixed layer depths. Other statistics of convection and cloudiness also vary with mixed layer depth. Figure 5 shows a great reduction of cloud fraction for the 50 m case (in black) compared to the 1 m case (in red), though both exceed the RCE result (in blue). Associated with this reduction is a small increase in SST and a significant decrease in the surface fluxes accompanied by an increase (by 4.2 W m^{-2}) in the SW absorbed at the surface, and a decrease in the downwelling LW due to weaker convective clouds and, therefore, a reduction in column net radiative heating (Table 1).

While we have no explanation for the specific difference between the 50 m case and the others shown in Figure 4, the fact that differences appear between simulations overall is not entirely surprising. Multiple equilibria for identical boundary conditions and forcings have been observed in WTG simulations with many different models [*Sobel et al.*, 2007; *Sessions et al.*, 2010; *Daleu et al.*, 2015] even over fixed SST; ocean coupling adds an additional degree of freedom, and it is plausible that this might enhance, or at least not diminish the tendency for multiple equilibria to occur. The differences between the 50 m case and the others are not due to convective self-aggregation [e.g., *Bretherton et al.*, 2005; *Wing and Emanuel*, 2014] as this does not occur on our small computational domain. Snapshots of OLR or precipitation (not shown) show disorganized fields of convection in all simulations presented in this study.

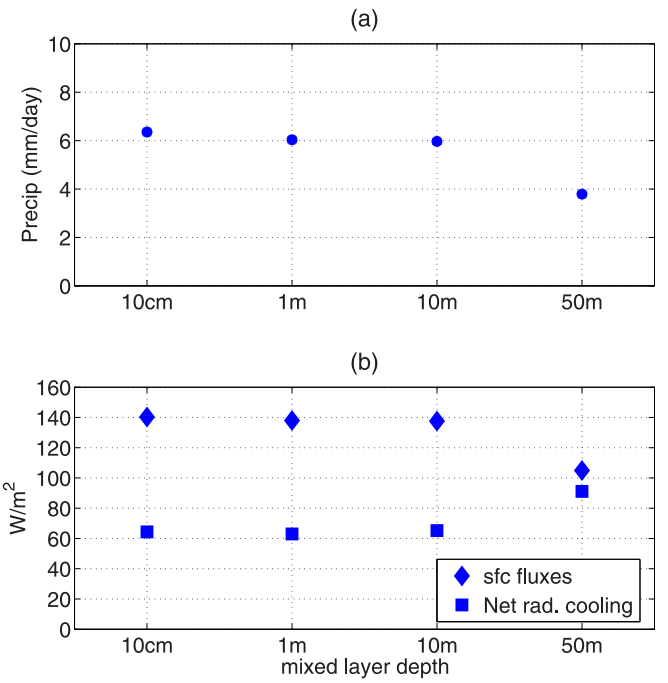

Figure 4. Time-averaged (a) precipitation and (b) diabatic energy sources: surface turbulent fluxes (diamonds), and column-integrated radiative cooling (squares) as a function of the mixed layer depth for the unsheared environment in the WTG runs.

The normalized gross moist stabilities of the time-averaged states are 1.7 for the cases of H =10 cm, 1 m, and 10 m, and 0.46 for the case of H = 50 m. In the 50 m case, the difference between the surface fluxes and radiative cooling is small, as shown in Figure 4b. Thus the implied MSE export is small, and since the gross moist stability remains significantly greater than zero, the precipitation is

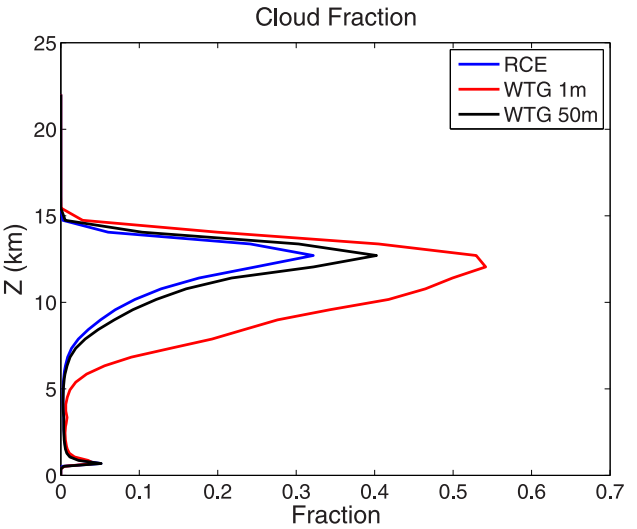

Figure 5. Cloud fraction for the RCE experiment (blue), the unsheared WTG experiment with $H = 1$ m (red), and unsheared WTG experiment with $H = 50$ m (black). The $H = 10$ cm and 10 m cases are very similar to the 1 m case and are not shown.

close to the surface evaporation. Essentially, this solution is close to RCE, though it did not need to be by construction.

3.2. Properties of the Coupled System in a Sheared Environment

3.2.1. Case of H = 1 m

In the experiments discussed above, the time series of rain rate (not shown) are approximately constant in time, indicating stable precipitating equilibria. When the environment is sheared, similar behavior is found for the smaller values of shear. However, for a given H, there exists a shear strength above which regular oscillations occur between precipitating and dry states. In particular, given a mixed layer of 1 m depth, for a vertical shear of 30 m s^{-1} over 12 km (but not smaller shears, the next smallest tried being 20 m s^{-1}), such behavior occurs, as shown in Figure 6. Such strong shear has been observed during the active phase of the MJO in the Indian Ocean [e.g., *Johnson and Ciesielski*, 2013; *Sobel et al*., 2014] when the low level westerlies reach 15 m s^{-1} while the upper level easterlies exceed 20 m s^{-1}.

Figure 6a shows pulse-like oscillations in precipitation, in which a few rainy days, with peak rainfall rates around 20 mm d^{-1}, are followed by approximately 10 dry days. Surface turbulent fluxes (Figure 6b) vary more gradually, and are nearly in phase with precipitation, though the surface flux maxima slightly lag the rainfall maxima. Atmospheric column net radiative heating (Figure 6c) is out of phase with precipitation, with minima before (and during) the onset of precipitation, and broad maxima following and extending much longer than the rainy periods and well into the dry periods. Variations in column water vapor (Figure 6g) resemble those in radiative heating. SST (Figure 6f) oscillates between a cold state reaching 296 K and a briefer warm state where maxima reach approximately 301 K. The oscillations in SST are driven by variations in surface turbulent fluxes and surface insolation (Figure 6d), both of which show oscillations on the order of 200 W m^{-2} in amplitude.

Inspection of the large-scale vertical motion in Figure 7 shows a transition from a first to a second baroclinic mode structure up to the upper troposphere about 12 km, as the rainy phase of the oscillation proceeds. As discussed in a recent study [*Anber et al*., 2016], this thick stratiform anvil is a result of cloud-radiation interaction, which leads to the second baroclinic mode response in the large-scale vertical velocity and associated increase in gross moist stability, which acts to reduce precipitation. However, in *Anber et al*. [2016], feedback from the surface was completely eliminated by prescribing the sensible and latent heat fluxes. In our simulations here, the surface is allowed to respond to the changes in surface turbulent and radiative fluxes. In response to the decrease in the absorbed shortwave radiation at the surface due to blocking from the anvil stratiform clouds, as well as the increased surface latent heat flux, the SST drops during the rainy phase. Since the free-tropospheric temperature profile is held nearly constant under via WTG, the reduced SST stabilizes the column and shuts down convection, leading to large-scale radiatively driven descent which in

Table 1. Surface Energy Budget Terms of Equation (1) for RCE and WTG, H = 1 m, and H= 50 m Simulations: Sea Surface Temperature (SST) in K, Surface Turbulent Fluxes (Latent + Sensible), Absorbed (Downward − Upward) Shortwave (SW), Upward Longwave (LW↑), and Downward Longwave (LW↓) in W m^{-2}

	SST	Sfc Fluxes	$SW_{absorbed}$	LW↓	LW↑
RCE	299.75	110.14	200.62	358.14	448.61
WTG, H = 1 m	299.95	137.38	223.28	363.91	449.81
WTG, H = 50 m	300.72	113.46	227.45	340.45	454.45

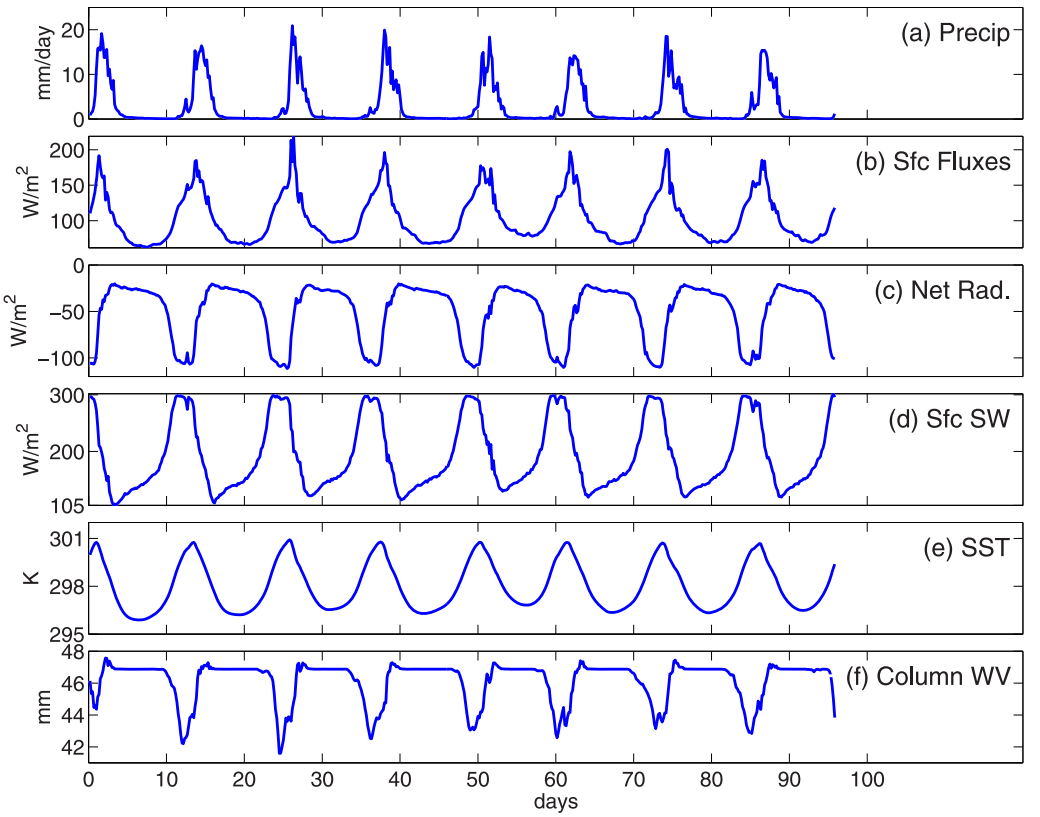

Figure 6. Time series of domain-averaged (a) precipitation in mm d^{-1}, (b) surface fluxes (latent + sensible), (c) net radiative cooling, (d) absorbed shortwave flux at the surface (incident minus reflected), (e) SST in K, and (f) column water vapor in mm. These results are from the case with a mixed layer depth of 1 m and mean shear strength 30 m s^{-1} over 12 km.

turn dries the troposphere. As the mixed layer temperature (SST) gradually recovers due to increasing shortwave at the surface during the dry phase, eventually reaching a critical value, deep convection is reactivated. This cycle is qualitatively similar to that found by SG03, but here the convection is explicitly modeled rather than highly parameterized; radiative and surface turbulent fluxes are represented separately by much more realistic parameterizations; and the onset of oscillatory behavior here is controlled by vertical shear, which was not represented at all in the model of SG03.

3.2.2. Case of H = 10 m

Figure 8 shows results in the same format as Figure 6, but with a mixed layer depth of 10 m. The period of oscillations is approximately 50 days, and the recovery of the surface during the suppressed phase is much more gradual than in the H =1 m case. This reduction in frequency is an expected consequence of the increased heat capacity of the deeper mixed layer.

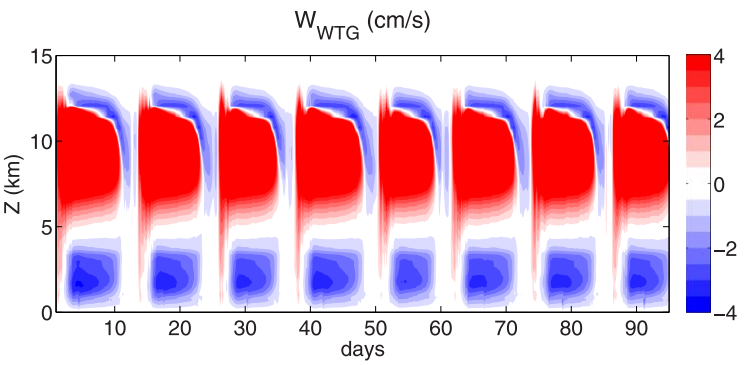

Figure 7. Time series of the large-scale vertical velocity W_{WTG} for the case of mixed layer depth 1 m, and shear strength 30 m s^{-1} over 12 km.

The mixed layer temperature shows nonlinear oscillations. Its recovery after cooling is characterized by two quasi-linear stages: an overcast stage, similar to that identified in the 1 m mixed layer case, lasting about 10 days, during which the cloud and radiation

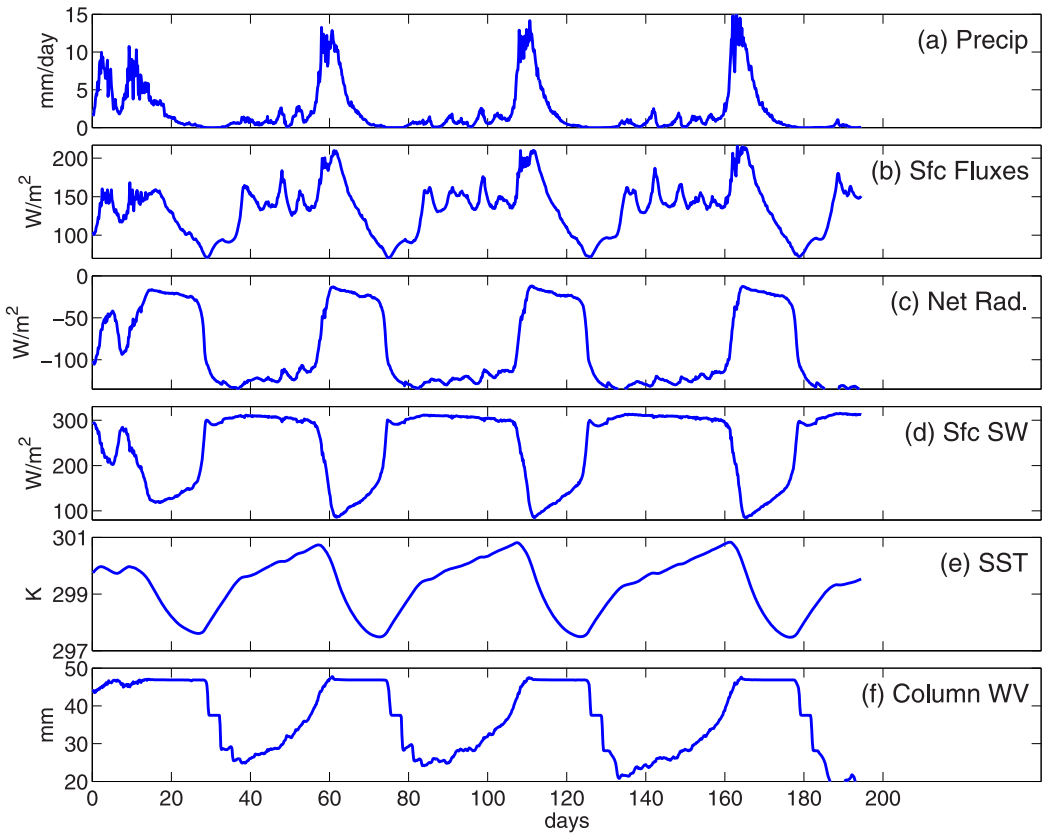

Figure 8. As Figure 6, but for a mixed layer of depth 10 m.

perturbations associated with the rainy phase gradually dissipate; and a second stage, lasting about 20 days, during which precipitation is only 1–2 mm d^{-1}, column net radiative cooling is nearly constant (about −120 W m^{-2}), and surface fluxes are sustained at 150 W m^{-2}. The second stage is absent in the 1 m mixed layer depth case.

Column water vapor varies over a much larger range than in the 1 m case, from ∼25 mm in the dry period to ∼47 mm in the wet periods. The time scale of column water vapor recovery is more than 20 days, during which precipitation is small and net radiative cooling is nearly constant. The large-scale vertical velocity (not shown) is descending, suggesting that vertical advective drying is responsible for the slow recovery of column water vapor and precipitation despite that the surface latent heat flux is not particularly small.

The oscillations here are similar to those found in SG03 and MS04, but those studies, unlike our here, did not consider the effects of vertical shear. The oscillatory behavior in the coupled system in our simulations appears only if three ingredients are present: coupling of a mixed layer slab ocean of sufficient depth, strong vertical shear, and interactive radiation (no oscillations occur when radiative feedbacks are disabled, for any magnitude of vertical shear or mixed layer depth). We performed experiments in which only two of the three factors exist and no oscillatory behavior was found.

The role of the mixed layer depth was a focus of SG03 and MS04. These studies found that there was an optimal mixed layer depth, on the order of 10–20 m, for which the oscillations were strongest. For either greater or smaller mixed layer depths, the oscillations' amplitudes (or growth rates, in the case of the linear model in SG03) decreased, vanishing altogether for sufficiently small values. In addition to the results shown above, we performed simulations (not shown) with a very shallow (H = 10 cm) mixed layer, and found no oscillations, in agreement with SG03 and MS04. When the mixed layer is very shallow, insignificantly small heat storage causes the SST to adjust very quickly to any change in the atmosphere. If convection is strong the SST will cool quickly due to reduced surface shortwave and increased latent heat flux, while if convection is absent the SST will warm quickly due to the opposite anomalies. The oscillations require SST to

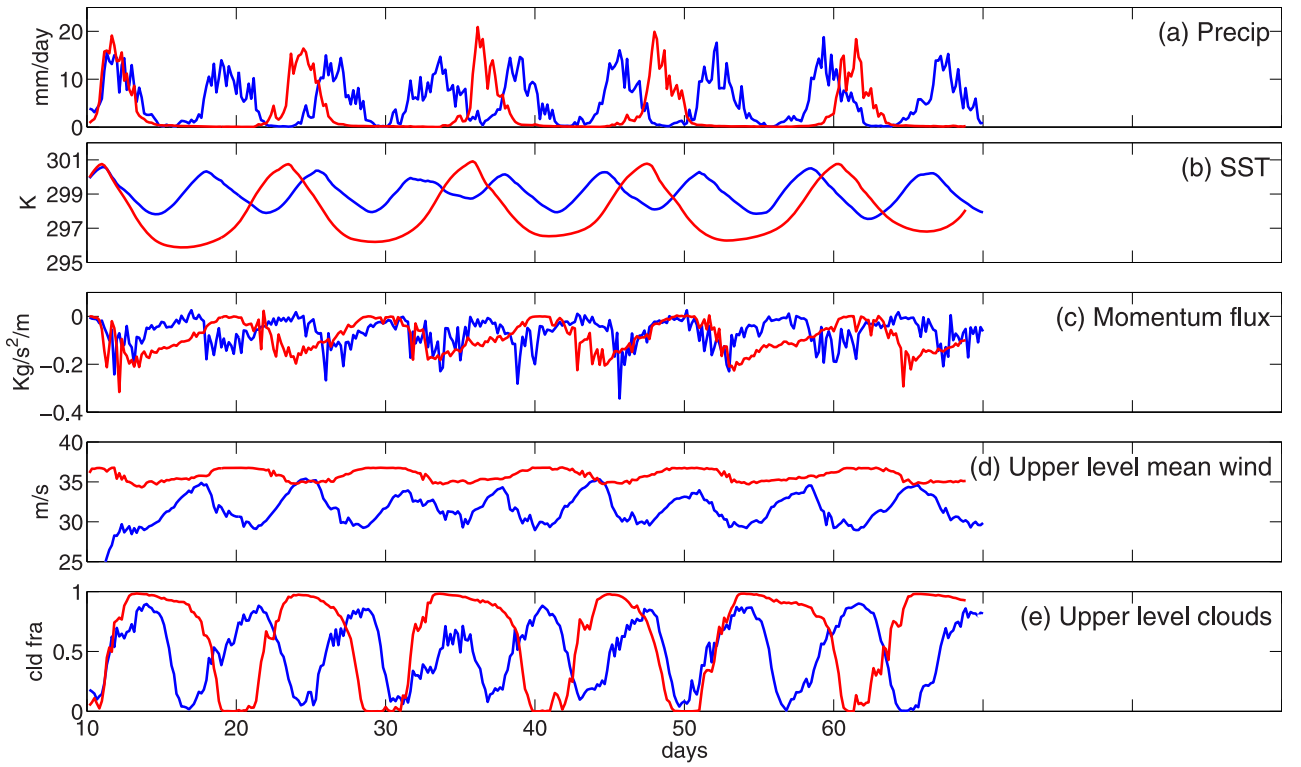

Figure 9. Time series of domain-averaged (a) precipitation, (b) SST, and (c) momentum fluxes averaged over 5–12 km, (d) upper levels mean zonal wind (e) cloud fraction, both averaged over 10–12 km for $H = 1$ m and wind shear of strength 40 m s^{-1} over 12 km, relaxation time scale of 1 day (blue). Same case but for relaxation time of 1 h is in red for comparison.

anomalies to be sustained for days in the presence of surface flux anomalies that oppose them, and this requires sufficient surface heat capacity. We also performed simulations (not shown) with a very deep (H = 500 m) mixed layer, and found no oscillations in that case either, in qualitative agreement with SG03. This indicates that, consistent with SG03, there is an optimal mixed layer depth where oscillations are strongest. This is also qualitatively consistent with our finding that smaller vertical wind shear is sufficient for the oscillations' development for the H = 10 m case—in which oscillations occur at a shear of 15 m s^{-1} over 12 km—than in the others shown above, though we did not attempt to determine the precise value of shear at which the onset of oscillations occurs.

We also performed experiments in which the shear relaxation time scale was altered from 1 h to 1 day. In this case, the oscillations' period decreased from 10 days (for the case of H = 1 m) to about 7 days as shown in Figures 9a, and 9b for SST and precipitation, respectively. In this case, convective momentum transport now ($\overline{\rho u' w'}$) is able to more substantially weaken the mean shear (shown in Figure 9d as upper level mean zonal wind averaged over 10–12 km), which in turn causes the anvil stratiform to be less persistent. Anvil stratiform is shown in Figure 9e as upper level cloud fraction averaged over 10–12 km, and momentum transport, defined as $\overline{\rho u' w'}$, is shown in Figure 9c averaged over 5–12 km, where ρ, u, and w, are the density, zonal wind, and vertical velocity, respectively, and primes are anomalies from the horizontal mean, and overbar is the horizontal mean.

4. Summary

We have presented results from simulations in which a slab ocean mixed layer is coupled to atmospheric convection in the idealized framework of a three-dimensional cloud-resolving model with parameterized large-scale circulation with imposed vertical shear. The mixed layer depth and vertical shear magnitude are varied as control parameters.

First, we performed a radiative-convective equilibrium experiment in which the atmosphere was coupled to a slab ocean of a mixed layer 1 m deep and forced by a global average solar insolation in the absence of

vertical shear to obtain equilibrium atmospheric and surface states. Then, experiments were performed in the WTG mode with initial conditions and the atmospheric target profile taken from the RCE run, but greater insolation to drive mean ascent, such as is observed in regions of large MJO amplitude in convection, was imposed. Despite the increase in solar insolation by over 90 W m^{-2}, time mean sea surface temperature remained almost unchanged, primarily due to the negative cloud shortwave feedback induced by the stronger deep convection, as the time mean precipitation and vertical motion increased substantially.

When vertical wind shear of sufficient magnitude is introduced, the coupled system exhibits oscillations between wet and dry periods, with varying frequencies depending on the depth of the mixed layer. Cloud-radiation feedback, vertical wind shear, and a slab ocean mixed layer are all necessary (but not sufficient) ingredients for these oscillations to occur; in the absence of any of these components, the system attains a nonoscillatory, more nearly steady state.

The conditions necessary to induce oscillations in our calculations are not difficult to find in nature. During the recent field program Cooperative Indian Ocean Experiment on Intraseasonal Variability (CINDY)/Dynamics of the MJO (DYNAMO) [e.g., *Wang et al*., 2015, 2016; *Yoneyama et al*., 2013], all three conditions were observed during the MJO events: a deep layer of vertical wind shear reaching 30 m s^{-1} over the troposphere during the MJO active phases [e.g., *Johnson and Ciesielski*, 2013], strong cloud-radiative feedback [*Sobel et al*., 2014], and a relatively deep ocean mixed layer [e.g., *Chi et al*., 2014]. Hence, the results from our idealized CRM experiments may be relevant to the observed MJO.

Acknowledgments
This research was supported by NSF grants AGS-1008847 and AGS-1543932. The simulations were performed on YETI cluster at Columbia University. The program code for the simulations, based on the Weather Research and Forecast (WRF) model, and the simulation outputs are available from the first author (uanber@princeton.edu) upon request.

References

Anber, U., S. Wang, and A. Sobel (2014), Response of atmospheric convection to vertical wind shear: Cloud resolving simulations with parameterized large-scale circulation. Part I: Specified radiative cooling, *J. Atmos. Sci.*, *71*, 2976–2993.

Anber, U., S. Wang, and A. Sobel (2015), Effect of surface fluxes versus radiative heating on tropical deep convection, *J. Atmos. Sci.*, *72*, 3378–3388.

Anber, U., S. Wang, and A. Sobel (2016), Response of atmospheric convection to vertical wind shear: Cloud resolving simulations with parameterized large-scale circulation. Part II: Effect of interactive radiation, *J. Atmos. Sci.*, *73*, 199–209.

Andersen, J. A., and Z. Kuang (2012), Moist static energy budget of MJO-like disturbances in the atmosphere of a zonally symmetric aqua-planet, *J. Clim.*, *25*, 2782–2804.

Bretherton, C. S., and P. K. Smolarkiewicz (1989), Gravity waves, compensating subsidence and detrainment around cumulus clouds, *J. Atmos. Sci.*, *46*, 740–759.

Bretherton, C. S., P. N. Blossey, and M. Khairoutdinov (2005), An energy-balance analysis of deep convective self-aggregation above uniform SST, *J. Atmos. Sci.*, *62*, 4273–4292.

Chen, S.-H., and W.-Y. Sun (2002), A one-dimensional time dependent cloud model., *J. Meteor. Soc. Japan*, *80*, 99–118, doi:10.2151/jmsj.80.99.

Chi, N.-H., R.-C. Lien, E. A. D'Asaro, and B. B. Ma (2014), The surface mixed layer heat budget from mooring observations in the central Indian Ocean during Madden-Julian Oscillation events, *J. Geophys. Res. Oceans*, *119*, 4638–4652, doi:10.1002/2014JC010192.

Collins, W. D., et al. (2004), Description of the NCAR Community Atmosphere Model: CAM 3.0, *Tech. Rep. NCAR/TN-464+STR*, 226 pp. [Available online at http:// www.cesm.ucar.edu/models/atm-cam/docs/description/ description.pdf.]

Cronin, T. W., and K. A. Emanuel (2013), The climate time scale in the approach to radiative-convective equilibrium, *J. Adv. Model. Earth Syst.*, *5*, 843–849, doi:10.1002/jame.20049.

Daleu, C. L., et al. (2015), Intercomparison of methods of coupling between convection and large-scale circulation: 1. Comparison over uniform surface conditions, *J. Adv. Model. Earth Syst.*, *7*, 1576–1601, doi:10.1002/2015MS000468.

Emanuel, K., A. A. Wing, and E. M. Vincent (2014), Radiative-convective instability, *J. Adv. Model. Earth Syst.*, *6*, 75–90, doi:10.1002/2013MS000270.

Hohenegger, C., and B. Stevens (2016), Coupled radiative convective equilibrium simulations with explicit and parameterized convection, *J. Adv. Model. Earth Syst.*, *8*, 1468–1482, doi:10.1002/2016MS000666.

Hong, S.-Y., and H.-L. Pan (1996), Nonlocal boundary layer vertical diffusion in a medium-range forecast model, *Mon. Wea. Rev.*, *124*, 2322–2339, doi:10.1175/1520-0493(1996)124,2322:NBLVDI.2.0.CO;2.

Hong, S.-Y., Y. Noh, and J. Dudhia (2006), A new vertical diffusion package with an explicit treatment of entrainment processes, *Mon. Wea. Rev.*, *134*, 2318–2341, doi:10.1175/MWR3199.1.

Johnson, R. H., and P. E. Ciesielski (2013), Structure and properties of Madden–Julian oscillations deduced from DYNAMO sounding arrays, *J. Atmos. Sci.*, *70*, 3157–3179.

Kim, D., A. H. Sobel, and I.-S. Kang (2011), A mechanism denial study on the Madden-Julian oscillation, *J. Adv. Model. Earth Syst.*, *3*, M12007, doi:10.1029/2011MS000081.

Klemp, J. B., J. Dudhia, and A. D. Hassiotis (2008), An upper gravity-wave absorbing layer for NWP applications, *Mon. Wea. Rev.*, *136*, 3987–4004, doi:10.1175/2008MWR2596.1.

Maloney, E., and A. Sobel (2004), Surface fluxes and ocean coupling in the tropical intraseasonal oscillation, *J. Clim.*, *17*, 4368–4386, doi:10.1175/JCLI-3212.1.

Neelin, J. D., and I. M. Held (1987), Modeling tropical convergence based on the moist static energy budget, *Mon. Weather Rev.*, *115*, 3–12.

Neelin, J. D., and N. Zeng (2000), A quasi-equilibrium tropical circulation model—formulation, *J. Atmos. Sci.*, *57*, 1741–1766.

Noh, Y., W. G. Cheon, S. Y. Hong, and S. Raasch (2003), Improvement of the K-profile model for the planetary boundary layer based on large eddy simulation data, *Bound.-Layer Meteor.*, *107*, 401–427, doi:10.1023/A:1022146015946.

Raymond, D. J. (2001), A new model of the Madden–Julian oscillation, *J. Atmos. Sci.*, *58*, 2807–2819.

Raymond, D. J., and X. Zeng (2005), Modelling tropical atmospheric convection in the context of the Weak Temperature Gradient approximation, *Q. J. R. Meteorol. Soc.*, *131*, 1301–1320.
Raymond, D. J., S. Sessions, A. H. Sobel, and Z. Fuchs (2009), The mechanics of gross moist stability, *J. Adv. Model. Earth Syst.*, *1*, 9, doi: 10.3894/JAMES.2009.1.9.
Sessions, S., S. Sugaya, D. J. Raymond, and A. H. Sobel (2010), Multiple equilibria in a cloud-resolving model, *J. Geophys. Res.*, *115*, D12110, doi:10.1029/2009JD013376.
Sobel, A., and H. Gildor (2003), A simple time-dependent model of SST hot spots, *J. Clim.*, *16*, 3978–3992.
Sobel, A., S. Wang, and D. Kim (2014), Moist static energy budget of the MJO during DYNAMO, *J. Atmos. Sci.*, *71*, 4276–4291.
Sobel, A. H., G. Bellon, and J. Bacmeister (2007), Multiple equilibria in a single-column model of the tropical atmosphere, *Geophys. Res. Lett.*, *34*, L22804, doi:10.1029/2007GL031320.
Sobel, A. H., E. D. Maloney, G. Bellon, and D. M. Frierson (2008), The role surface heat fluxes in tropical intraseasonal oscillations, *Nat. Geosci.*, *1*, 653–657.
Sobel, A. H., E. D. Maloney, G. Bellon, and D. M. Frierson (2010), Surface fluxes and tropical intraseasonal variability: A reassessment, *J. Adv. Model. Earth Syst.*, *2,2*, doi:10.3894/JAMES.2010.2.2.
Stephens, G. L., P. J. Webster, R. H. Johnson, R. Engelen, and T. L'Ecuyer (2004), Observational evidence for the mutual regulation of the tropical hydrological cycle and tropical sea surface temperatures, *J. Clim.*, *17*, 2213–2224.
Vecchi, G. A., and D. E. Harrison (2002), Monsoon breaks and subseasonal sea surface temperature variability in the Bay of Bengal, *J. Clim.*, *15*, 1485–1493.
Waliser, D. E. (1996), Formation and limiting mechanisms for very high sea surface temperature: Linking the dynamics and the thermodynamics, *J. Clim.*, *9*, 161–188.
Wang, S., and A. H. Sobel (2011), Response of convection to relative sea surface temperature: Cloud-resolving simulations in two and three dimensions, *J. Geophys. Res.*, *116*, D11119, doi:10.1029/2010JD015347.
Wang, S., A. H. Sobel, F. Zhang, Y. Q. Sun, Y. Yue, and L. Zhou (2015), Regional simulation of the October and November MJO events observed during the CINDY/DYNAMO field campaign at gray zone resolution, *J. Clim.*, *28*, 2097–2119.
Wang, S., A. H. Sobel, and J. Nie (2016), Modeling the MJO in a cloud-resolving model with parameterized large-scale dynamics: Vertical structure, radiation, and horizontal advection of dry air, *J. Adv. Model. Earth Syst.*, *8*, 121–139, doi:10.1002/2015MS000529.
Wing, A. A., and K. A. Emanuel (2014), Physical mechanisms controlling self-aggregation of convection in idealized numerical modeling simulations, *J. Adv. Model. Earth Syst.*, *6*, 59–74, doi:10.1002/2013MS000269.
Woolnough, S. J., J. M. Slingo, and B. J. Hoskins (2000), The relationship between convection and sea surface temperature on intraseasonal timescales, *J. Clim.*, *13*, 2086–2104.
Yoneyama, K., C. Zhang, and C. N. Long (2013), Tracking pulses of the Madden-Julian oscillation, *Bull. Am. Meteorol. Soc.*, *94*, 1871–1891, doi:10.1175/BAMS-D-12-00157.1.